Macromolecules

pubs.acs.org/Macromolecules Article

Impact of Processing Effects on Surface Segregation of Bottlebrush Polymer Additives

Dongjoo Lee, Nilesh Charpota, Hao Mei, Tanguy Terlier, Danica Pietrzak, Gila E. Stein,* and Rafael Verduzco*

Cite This: https://doi.org/10.1021/acs.macromol.2c01418 Read Online

ACCESS | Metrics & More | Article Recommendations | Supporting Information

ABSTRACT: The surface properties of polymeric materials govern interactions with the surroundings and are responsible for various application-relevant properties. Recent studies have shown that bottlebrush polymers can be used to modify the surface chemistry of the polymers because they spontaneously segregate to the interfaces when they are blended with the linear polymers, driven in large part by entropic effects that arise from the unique architecture of bottlebrush polymers. However, while prior work has largely focused on equilibrium segregation profiles, kinetic and processing effects can also drive bottlebrush additives to surfaces and interfaces. In solution-cast blends of polymers and colloids, vertical stratification is controlled by the relative Péclet (*Pe*) numbers of the constituents, i.e., the relative rates of solvent evaporation and solute diffusion. Herein, we studied processing effects that drive bottlebrush additives to interfaces when blended with linear polymers. We prepared blends of bottlebrush polystyrene (BBPS) and linear perdeuterated polystyrene (dPS), where the BBPS side-chain length was fixed at N_{sc} = 48, the BBPS backbone length ranged from N_b = 30−260, and the dPS chain length ranged from N_m = 40−548. The relative *Pe* numbers of BBPS and dPS were varied by changing the solvent and sizes of BBPS and dPS. In contrast to other binary blends where the constituents have disparate sizes (e.g., colloid/colloid, polymer/colloid, and polymer/polymer), we found that the relative *Pe* number cannot account for the degree of segregation observed in these bottlebrush and linear polymer blends. For a fixed BBPS side-chain length, we observe stronger surface segregation of bottlebrush additives when the blend is cast using lower boiling point solvents and/or for blends with longer bottlebrush polymers. We further show that solvent annealing of the film can increase the enrichment of bottlebrush additives near surfaces. This study provides insight into the interplay of processing effects and blend thermodynamics that govern surface segregation of bottlebrush polymer additives.

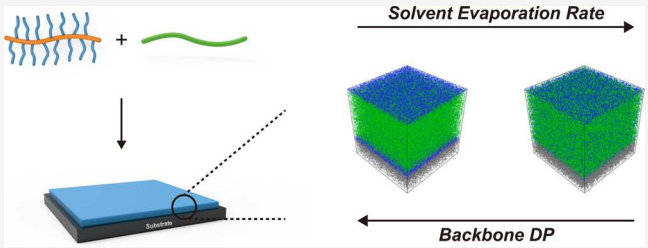

■ INTRODUCTION

The surface properties of polymeric materials govern interactions with the surroundings and are responsible for various application-relevant properties such as adhesion, wettability, and fouling resistance.[1,2] As a result, a variety of methods have been developed for modifying surfaces and interfaces. However, many of these methods involve additional processing or treatment steps.[2−5] For example, polymers can be tethered to a surface through surface-initiated polymerization reactions,[6,7] and other approaches include plasma treatment,[8,9] vapor-initiated growth,[10,11] and chemical modifications, such as through polydopamine polymerization on a surface.[12]

The use of surface-active additives provides an alternative and potentially simpler approach to modifying surface properties, as the additives spontaneously migrate to surfaces without additional processing steps. For example, Asatekin et al. used polyacrylonitrile-*graft*-poly(ethylene oxide) (PAN-*g*-PEO), an amphiphilic comb copolymer, to modify the surface of ultrafiltration membranes. They showed that the amphiphilic comb copolymer additives segregated to the surface of the membranes and increased hydrophilicity.[13] In another study, Maguire and co-workers studied the surface segregation of poly(methyl methacrylate) (PMMA)-grafted silica nanoparticles from a poly(styrene-*ran*-acrylonitrile) matrix. They showed that PMMA-grafted silica nanoparticles, which have a lower surface energy compared to poly(styrene-*ran*-acrylonitrile), rapidly wet the free surface during thermal annealing.[14] Other examples of surface-active additives include polymer-grafted gold nanoparticles[15] and surfactants,[16−18] and general strategies for tailoring the attraction of polymers to interfaces and modifying polymeric surfaces are described in recent reviews.[1,2]

Several studies have examined the thin film structure in blends of bottlebrush and linear homopolymers. A variety of

Received: July 8, 2022
Revised: September 10, 2022

systems were considered, including blends where enthalpic interactions between the bottlebrush and linear polymer were approximately athermal,[19,20] attractive,[21] or repulsive.[22] The surface energies of the bottlebrush and linear polymer were always similar. In these cases, the bottlebrush polymers could spontaneously segregate to the interfaces when $N_m/N_{sc} > 2$, consistent with an entropic preference for chain ends near the surface.[19,20] The extent of the segregation was controlled by architectural parameters (N_b, N_{sc}, N_m) as well as the strength of enthalpic interactions in the bulk and at the surfaces.[1,19,20,22−24] Bottlebrush additives could therefore be used to tune the hydrophilicity of a surface[22,25] or introduce novel chemistries at a polymer surface, even when side chains have higher cohesive energy densities than the matrix.[21]

The role of entropic effects in driving surface segregation is not unique to blends of bottlebrush and linear polymers, and foundational studies have detailed the importance of entropic effects in a wide variety of polymer blends. For example, Yethiraj investigated athermal and thermal blends of branched and linear polymers using Monte Carlo simulations and showed that the branched polymers preferentially segregate to interfaces, if polymer−polymer enthalpic interactions were comparable to those between polymers and the interface.[26] These predictions were consistent with subsequent experiments, which demonstrated that branched polymer additives could be used to modify surface chemistry.[18,21] Other examples include the observation of polymer chain ends near interfaces and the preferential surface segregation of star or cyclic polymers, as described in recent reviews.[27,28] Bottlebrush polymers have unique advantages, which may be beneficial for the development of surface-active additives. Both the length of the side chains and the number of side chains per bottlebrush polymer can be controlled, and this is useful for performing fundamental studies focused on understanding the impact of architectural effects on surface segregation. Additionally, bottlebrush copolymers with mixtures of different side-chain chemistries are readily accessible. This attribute enables one to combine "functional" side chains and "compatibilizer" side chains in a single platform, as demonstrated in the use of bottlebrush polymers with poly(dimethylsiloxane) (PDMS) side chains to tailor the surface of poly(lactic acid) (PLA) films.[25]

Processing effects also play an important role in the segregation of bottlebrush additives to interfaces, but these remain poorly understood. Our prior work has shown that the segregation of bottlebrush polymers to the surface was strongest in as-cast films, i.e., immediately after solution deposition and without any thermal annealing, provided $N_m/N_{sc} > 2$. Some surface enrichment remained after thermal annealing, but the degree of surface enrichment decreased significantly relative to the as-cast films. This was observed for a variety of bottlebrush additives blended with linear polymers.[19,22−24] We speculated that the presence of solvent in the environment could play a role,[23] but a detailed study of processing effects was not performed.

Processing effects are well studied for other types of binary systems where the constituents have disparate sizes, such as colloid/colloid, polymer/colloid, and linear polymer/polymer systems.[29−36] These studies have shown that the ratio of the Péclet numbers of the constituents plays an important role in dictating surface enrichment in these blends. The *Pe* number describes the relative rates of solvent evaporation and solute diffusion:

$$Pe = \frac{6\pi\eta R_h HE}{kT}$$

where η is the solvent viscosity, R_h is the hydrodynamic radius of the particle, H is the initial film thickness, E is the rate of evaporation, k is the Boltzmann's constant, and T is the temperature. Solvent evaporation is faster than solute diffusion when *Pe* is greater than 1, and diffusion is faster than evaporation for *Pe* number less than 1. In general, studies of polymer and colloid blends have reported that the smaller solute is enriched at the surface when *Pe* numbers of both solutes are greater than 1 and that the degree of enrichment increases with increasing *Pe* number of the larger solute. For example, Fortini and co-workers studied colloid−colloid mixtures and found that the smaller solute enriched the surface ("small-on-top" stratification) when the *Pe* number for both particles was greater than 1.[32] In another study, Howard and co-workers studied polymer−polymer and colloid−polymer mixtures using Langevin dynamics.[35] For polymer−polymer mixtures, they found that shorter polymers were enriched near the surface and longer polymers were depleted from the surface, and this effect was more pronounced as the size of the shorter polymer decreased with that of the longer polymer held constant. Colloid−polymer mixtures also displayed similar trends. Smaller particles (either polymer or colloid) were enriched near the drying interfaces, and the solute with the larger *Pe* number was enriched in the bulk polymer film. However, these trends have not been studied for blends of bottlebrush polymers and linear polymers. Blends of bottlebrush polymers and linear polymers may show qualitatively different effects compared with polymer/polymer or polymer/colloid blends due to strong entropic effects arising from the unique bottlebrush architecture. These effects in general drive the bottlebrush toward surfaces and interfaces and may be relevant to processing-related effects that produce enrichment of bottlebrushes during casting. Architectural parameters such as N_b, N_m, and N_{sc} that govern the strength of entropic effects are expected to play a role along with other processing-specific variables, such as the rate of solvent evaporation and the film casting and annealing history.

Herein, we investigated the effects of processing on surface segregation of bottlebrush polymer additives by studying blends of BBPS with linear perdeuterated polystyrene (dPS), as shown in Figure 1. We varied the relative sizes of bottlebrush and linear polymer by systematically varying N_b and N_m while maintaining a constant N_{sc}. We found that non-equilibrium effects do play an important role in the surface enrichment of bottlebrush additives, and surface enrichment was in general stronger in blend films prior to thermal annealing. In contrast to prior studies of polymer and colloidal blends, where smaller solutes typically segregated at the surface when *Pe* numbers of both solutes are greater than 1, we found that the bottlebrush polymer additives with larger *Pe* number than the linear polymer host will segregate at the surface, provided that $N_m/N_{sc} > 2$, and segregation was stronger in as-cast films compared with thermally annealed films. We studied a series of blends and found variations in the segregation behavior even when controlling for the relative *Pe* number, indicating that the ratio of *Pe* numbers cannot account for the segregation behavior when bottlebrush polymers are present. Rather, entropic effects, dependent in part on the length of the bottlebrush backbone, dominated segregation behavior. We also found that vertical stratification increased with the

https://doi.org/10.1021/acs.macromol.2c01418
Macromolecules XXXX, XXX, XXX−XXX

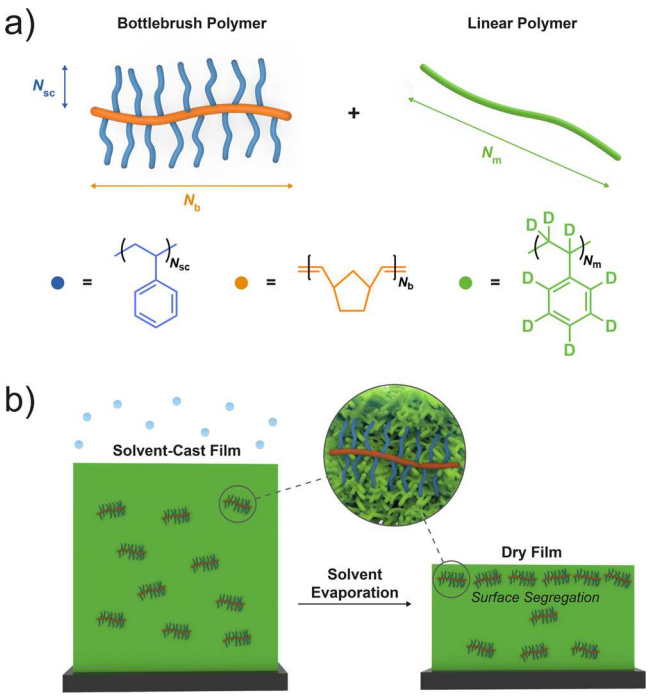

Figure 1. Schematic illustrations of the (a) bottlebrush polymer and linear polymer studied. The bottlebrush polymer contained polystyrene side chains, and these were blended with the linear polymer composed of perdeuterated polystyrene. The architectures of each are determined by the side-chain degree of polymerization N_{sc}, the backbone degree of polymerization N_b, and the linear polymer degree of polymerization N_m. (b) Vertical stratification of the bottlebrush/linear polymer blend during casting.

Table 1. Characteristics of Linear Perdeuterated Polystyrene (dPS), Macromonomer Polystyrene (NBPS), Bottlebrush Polystyrene (BBPS), and Bottlebrush Polystyrene-*co*-perdeuterated Polystyrene (BB(PS-*co*-dPS))

polymer	M_n (kg/mol)[a]	$Đ$[b]	DP	N_{sc}[c]	N_b[d]	ρ (%)[e]
Linear Polymers						
dPS40	4.50	1.48	40.1			
dPS205	23.0	1.07	205			
dPS548	61.5	1.02	548			
NBPS1	5.49	1.08	47.9			
NBPS2	4.60	1.04	39.3			
NBdPS	4.15	1.03	32.5			
Bottlebrush Polymers						
BBPS30	167	1.19		47.9	30.4	86.3
BBPS70	382	1.07		47.9	69.5	88.3
BBPS180	989	1.24		47.9	180.2	85.5
BBPS260	1425	1.18		47.9	259.6	90.2
BB(PS-*co*-dPS) 45	201	1.05		36.6[f]	45.4	93.8
BB(PS-*co*-dPS) 80	354	1.21		36.6[f]	80.1	97.1
BBPS146	645	1.04		39.3	146.0	93.3
BBPS350	1547	1.14		39.3	349.6	94.0

[a] M_n is the number-averaged molecular weight. Determined by ^{1}H NMR. [b] $Đ$ is the molecular-weight dispersity. Determined by GPC-RI analysis. [c] N_{sc} is the side-chain degree of polymerization. Determined by ^{1}H NMR. [d] N_b is the backbone degree of polymerization. Determined by the ratio of M_n of the BBPS to the M_n of the NBPS. [e] ρ indicates the conversion of the macromonomer. Conversion determined by GPC-RI analysis. [f] For bottlebrush polymers with PS and dPS side chains, N_{sc} represents the average side-chain degree of polymerization.

evaporation rate of the casting solvent. Similarly, we found that solvent annealing of blend films could increase segregation indicating that the presence of solvent during casting does play an important role in driving the segregation of bottlebrushes toward surfaces. This study provides new insights into factors that affect stratification when casting thin film blends and potentially provides a general route to tailor thin film surface properties using bottlebrush polymer additives.

■ EXPERIMENTAL SECTION

Materials. All chemical reagents were purchased from commercial sources and used as received unless noted otherwise. Silicon wafers were washed with Hellmanex III, deionized water, acetone, and isopropyl alcohol with sonication for 15 min for each solvent. Then, the wafers were treated with UV/ozone for 30 min to remove contaminants. 2,2′-Azobis(2-methylpropionitrile) (AIBN) was purified by recrystallization in methanol. Styrene and styrene-d_8 (Sigma-Aldrich Co., LLC) were passed through an alumina column to remove the inhibitor. *exo*-5-Norbornenecarboxylic acid (*exo*-NBCOOH) and third-generation Grubbs catalyst, ichloro[1,3-bis(2,4,6-trimethylphenyl)-2-imidazolidinylidene](benzylidene)bis(3-bromopyridine)-ruthenium(III), were purchased from Sigma-Aldrich Co., LLC. *exo*-5-Norbornene-2-methanol (*exo*-NBOH)[37] and ((1*S*,2*R*,4*S*)-bicyclo[2.2.1]hept-5-en-2-yl)methyl-4-cyano-4-(((dodecylsulfanyl)-carbonothioyl)-thio)-pentanoate (NBCTA)[22] were synthesized as previously reported. Linear dPS polymers were purchased from Polymer Source, Inc. (Table 1).

Norbornene-Functionalized Polystyrene Macromonomer (NBPS). NBPS was synthesized by reversible addition−fragmentation chain transfer (RAFT) polymerization as previously described, with modifications.[22] NBCTA (150.2 mg, 0.295 mmol), styrene (3.37 mL, 29.5 mmol), and AIBN (0.95 mg, 0.0059 mmol) were dissolved in 4 mL of anhydrous tetrahydrofuran (THF) in a Schlenk tube equipped with a stir bar. The Schlenk tube was degassed by three freeze−pump−thaw cycles. After the degasification step, the tube was heated to 80 °C to start the reaction. As the reaction progresses, aliquots were taken and tested by gel permeation chromatography (GPC) to monitor the molecular weight. After reaching the target molecular weight, the reaction was stopped by exposing the solution to the atmosphere. Then, the polymer was precipitated in cold methanol and collected by filtration. The polymer was dissolved in THF and reprecipitated in cold methanol two more times to further purify the macromonomer. 1H nuclear magnetic resonance (^{1}H NMR) and GPC analyses are presented in the Supporting Information, Figures S1 and S2, respectively.

Norbornene-Functionalized Perdeuterated Polystyrene Macromonomer (NBdPS). NBCTA (148.7 mg, 0.292 mmol), deuterated styrene (3.34 mL, 29.2 mmol), and AIBN (0.94 mg, 0.0058 mmol) were dissolved in 4 mL of anhydrous THF in a Schlenk tube equipped with a stir bar. The Schlenk tube was degassed by three freeze−pump−thaw cycles. After the degasification step, the tube was heated to 80 °C to start the reaction. As the reaction progresses, aliquots were taken and tested by GPC to monitor the molecular weight. After reaching the target molecular weight, the reaction was stopped by exposing the solution to the atmosphere. Then, the polymer was precipitated in cold methanol and collected by filtration. The polymer was dissolved in THF and reprecipitated in cold methanol two more times to further purify the macromonomer. GPC analysis is presented in the Supporting Information, Figure S3.

Bottlebrush Polystyrene (BBPS). BBPS was synthesized in a nitrogen-filled glove box. The predetermined amount of NBPS was added into a vial equipped with a stir bar. Anhydrous DCM was added to the vial targeting a total macromonomer concentration of 0.02 M. The pre-measured amount of third-generation Grubbs catalyst was dissolved in anhydrous DCM and was added into the vial

https://doi.org/10.1021/acs.macromol.2c01418
Macromolecules XXXX, XXX, XXX−XXX

(feed ratios of macromonomer to catalyst are shown in Table). After overnight reaction, the product was precipitated in cold methanol and collected by filtration. GPC analyses are presented in the Supporting Information, Figures S2 and S3.

Bottlebrush Polystyrene-co-perdeuterated Polystyrene (BB(PS-co-dPS)). BB(PS-*co*-dPS) was synthesized in a nitrogen-filled glove box. The predetermined amount of NBPS and NBdPS (NBPS:NBdPS = 6:4) was added into a vial equipped with a stir bar. Anhydrous DCM was added to the vial targeting a total macromonomer concentration of 0.02 M. The pre-measured amount of third-generation Grubbs catalyst was dissolved in anhydrous DCM and was added into the vial. After overnight reaction, the product was precipitated in cold methanol and collected by filtration. GPC analysis is presented in the Supporting Information, Figure S3.

Film Preparation. The bottlebrush polymer and linear polymer were dissolved in different casting solvents (chlorobenzene, toluene, 50/50 THF + toluene, and THF) at a total composition of 5 wt % solids. The mass ratio of bottlebrush polymer to linear polymer was 1:9 in all cases, and the mass ratio in binary bottlebrush blends was always 1:1. Films were cast by flow coating polymer blend solutions (15 μL) onto pre-cleaned silicon wafers.[38] The gap height was set as 200 μm for all films. Most film thicknesses ranged from 140 to 200 nm (Supporting Information, Tables S1−S5). Thermal annealing was performed inside a nitrogen-filled glovebox at 150 °C for 2 days.

Instrumentation. *GPC.* GPC was performed using an Agilent Technologies 1200 series module, with THF at 1 mL/min. The module was equipped with three PSS SDV columns in series (100, 1000, and 1000 Å pore sizes), an Agilent variable-wavelength UV/vis detector, a Wyatt Technology HELEOS II multiangle laser light scattering (MALLS) detector (λ = 658 nm), and a Wyatt Technology Optilab rEX refractive index (RI) detector. The flow rate of mobile-phase THF was 1 mL/min at 40 °C. The mass conversion of the bottlebrush polymer was calculated by comparing integrated RI peak areas for the bottlebrush polymer and macromonomer. The absolute molecular weight of the bottlebrush polymer was determined by static light scattering, and dn/dc was determined by RI analysis assuming 100% mass recovery of the bottlebrush polymer.

NMR Spectroscopy. ^{1}H NMR spectra were measured on Bruker 600 MHz spectrometers. ^{1}H NMR chemical shifts were reported in parts per million relative to internal solvent resonances.

Optical Microscopy (OM). Optical micrographs were captured by a Zeiss Axioplan 2 polarizing optical microscope operating in the reflectance mode.

Atomic Force Microscopy (AFM). AFM was performed using an NX20 atomic force microscope. The topography and phase contrast were measured by the tapping mode. The probes were silicon, with a spring constant of approximately 9 N/m and a resonant frequency of 115 kHz. The parameters used for image acquisition were 1.0 Hz scan frequency, 5 μm × 5 μm scan size, and 256 × 256 image resolution.

Time-of-Flight Secondary Ion Mass Spectrometry (ToF-SIMS). Positive high mass resolution depth profiling was performed using a ToF-SIMS NCS instrument, which combines a ToF.SIMS5 instrument (ION-TOF GmbH, Münster, Germany) and an in situ scanning probe microscope (NanoScan, Switzerland) and is maintained by the Shared Equipment Authority from Rice University. Bunched 30 keV Bi^{3+} ions (with a measured current of 0.2 pA) were used as primary probe for analysis (scanned area 100 × 100 μm^2), and sputtering was performed using Ar1500+ ions at 10 keV with a typical current around 0.7 nA, rastered area 500 × 500 μm^2. The beams were operated in non-interlaced mode, alternating one analysis cycle and one sputtering cycle (corresponding 1.63 s) followed by a pause of 5 s for charge compensation with an electron flood gun. An adjustment of the charge effects has been operated using a surface potential of 0 V and an extraction bias of 20 V. During the depth profiling, the cycle time was fixed to 200 μs (corresponding to m/z = 0−3649 amu mass range). All depth profiles have been point-to-point normalized by the total ion intensity, and the data have been plotted using a three-point adjacent averaging. Both normalization and smoothing have permitted a better comparison of the data from the different samples. The depth calibrations have been established based on the measured thicknesses using the surface profiler to obtain a line scan of the craters with the in situ scanning probe microscopy (SPM) by contact scanning.

Determination of Depth-Dependent Bottlebrush Polymer Compositions in Blend Films. The distribution of PS in blend films was determined through ToF-SIMS measurements. We used $C_7H_7^+$, $C_7D_7^+$, and Si^+ ion signals to track PS, dPS, and silicon, respectively. The distribution of BBPS in the linear dPS matrix was determined through calibration and measurement of the $C_7H_7^+/C_7D_7^+$ ion intensity ratio (Supporting Information). To calibrate ion intensity ratios, we measured the $C_7H_7^+/C_7D_7^+$ ion intensity ratio for a series of PS (M_n = 4.6 kg/mol) and dPS40 (M_n = 4.5 kg/mol) blends at known mass ratios. For each blend, we determined the average $C_7H_7^+/C_7D_7^+$ ion intensity ratio through ToF-SIMS. Then, we produced a linear fit of secondary ion intensity ratio as a function of PS mass composition and used this relation to determine the PS mass concentration based on measured secondary ion intensity ratios from the blend films. The resulting mass compositional distributions were integrated and normalized with respect to the known PS content in each film. The measured ion intensity ratios along with a linear fit to each dataset are presented in the Supporting Information, Table S6 and Figure S4.

Determination of Interfacial Excesses. The surface, substrate, and total excesses were determined through integration of the depth-dependent compositions of the bottlebrush polymers:

$$z^*_{surf} = \int_0^{h/2} [\varphi(z) - \varphi^0]\, dz$$

where surface excess is denoted as z^*_{surf}, h is the thickness of the film, z = 0 corresponds to the film−air interface, and $z = h$ corresponds to the film−substrate interfaces. $\varphi(z)$ is the weight fraction of the bottlebrush in the film as a function of depth z.

■ RESULTS AND DISCUSSION

The main goal of the study was to understand how processing conditions affect the surface segregation of the bottlebrush polymers in bottlebrush/linear polymer blends. We primarily studied blends of bottlebrush polymers with polystyrene side chains (BBPS) blended with linear dPS (Figure 1a). This blend system was chosen because these polymers have small differences in polymer cohesive energies, similar solubilities, and approximately neutral interactions.[19,20] We additionally studied some all-bottlebrush polymer blends, and to distinguish the bottlebrushes in the blends, one bottlebrush polymer was labeled with dPS side chains. The characteristics of these materials are provided in Table 1 and Supporting Information, Table S7. Across this series of samples, we varied N_m, N_b, the casting solvent used, and the post-deposition annealing conditions. We focus primarily on blends with $N_m/N_{sc} > 2$, except where indicated. Bottlebrush polymers with PS side chains or PS and dPS side chains were synthesized through a "grafting-through" ring-opening metathesis polymerization as shown in Supporting Information, Scheme S1. PS or dPS side chains were first synthesized by RAFT using an *exo*-norbornene-functionalized chain transfer agent (CTA). After synthesizing the macromonomers, bottlebrush polymers with varying backbone degree-of-polymerization N_b (30−350) were synthesized by ring-opening metathesis polymerization (ROMP). GPC analysis was used to confirm the high macromonomer conversion to bottlebrush polymer (Supporting Information, Figures S2 and S3).

First, we were interested in understanding whether the relative *Pe* numbers of bottlebrush polymer additive and linear polymer could predict enrichment or depletion at the surface, as has been observed in polymer/polymer, polymer/colloid, and colloid/colloid blends. We prepared a series of bottlebrush/linear polymer blends with systematically varying

https://doi.org/10.1021/acs.macromol.2c01418
Macromolecules XXXX, XXX, XXX−XXX

ratios of *Pe* numbers. Here, we define the *Pe* number ratio as that of the larger constituent to the smaller one, e.g., Pe_{BB}/Pe_{Linear}, where Pe_{BB} and Pe_{Linear} are the *Pe* numbers for the bottlebrush and linear polymers, respectively. We varied this ratio by varying the backbone length of the bottlebrush polymers (N_b = 30−260) (Table 1) while keeping the lengths of the linear polymer and bottlebrush side chains constant (dPS205, DP = 205, N_m/N_{sc} = 4.3). The *Pe* values for each polymer were determined by using viscometry to estimate the hydrodynamic radius of the linear polymer (R_h = 4.9 nm) and bottlebrush polymers (R_h = 7.1−16.1 nm). We assumed that the solvent evaporation rate was the same for these blends, as each solution contained the same linear polymer (dPS205), which comprised 90 wt % of solids in each solution. For the blends, the weight fraction of the BBPS was 10 wt %, and we analyzed both as-cast and thermally annealed (2 days at 150 °C) films. We used both OM (Supporting Information, Figures S5 and S6) and AFM (Supporting Information, Figures S7 and S8) to verify the uniformity of the films after casting. ToF-SIMS was used to determine the distribution of the BBPS throughout the films. Uncalibrated depth profiles for all blend film samples (uncalibrated intensity versus sputter time) are presented in the Supporting Information, Figures S9 and S10. In the main manuscript, we focus exclusively on segregation of the bottlebrush polymers toward the film−air interface, at film depth = 0%. Bottlebrush polymers also segregated toward the film−substrate interface. Full-depth profiles for all blend films and film thicknesses are provided in the Supporting Information.

In contrast to prior studies of solution-processed binary blends, which have reported stronger surface enrichment for the solute with smaller *Pe*, we observed enrichment of the bottlebrush polymer in all cases. To quantify the segregation of the bottlebrush polymers with varying N_b, we calculated the surface excess of the BBPS for each case (Figure 2b), and this shows that the surface excess of the BBPS increased with the number of backbone repeat units N_b, or equivalently, with increasing *Pe* ratio (Pe_{BB}/Pe_{Linear}). In contrast, after thermal annealing of the films for 2 days, we observed a measurable but much weaker surface enrichment of the bottlebrush. A representative depth profile after thermal annealing (N_b = 260) is shown in Figure 2a, and depth profiles for all blend films after annealing are provided in the Supporting Information, Figure S11. This observation is consistent with prior studies[1,19,20,22−24] and indicates that the strong surface enrichment observed in as-cast films is due in large part to processing effects during casting.[19,22,23]

To understand the role of the ratio of the Péclet numbers on surface enrichment in blend films, we prepared blends of either bottlebrush and linear polymer (blends 1 and 2) or two different bottlebrush polymers (blends 3 and 4). Across all of these blends, the ratio of the *Pe* numbers (Pe_{large}/Pe_{small}) was approximately 2.1 (Table 2). This ratio is arbitrary and chosen out of convenience, and we note that prior studies of stratification in colloidal or polymer−colloid blends have generally focused on larger *Pe* ratios (>4).[32,39,40] We cast each of these blends using either a high boiling point solvent (chlorobenzene), a moderate boiling point solvent (toluene), or a low boiling point solvent (THF) and analyzed the depth-dependent film concentration using ToF-SIMS to quantify the surface excess of the larger constituent. The surface excess of the larger constituent in the blend is shown in Figure 3, and uncalibrated depth profiles are presented in the Supporting Information, Figure S12. Both OM and AFM were used to verify the uniformity of the films, and these data are provided in the Supporting Information, Figures S13 and S14. In contrast to other binary blend systems (e.g., colloid/colloid, polymer/colloid, and polymer/polymer), the blends of the bottlebrush and linear polymers clearly showed segregation of the larger constituent (bottlebrush polymer) toward the film−air surface. Of the four blends shown in Table 2, the surface excess of the bottlebrush polymer was highest for blend 2, which contained the highest N_m/N_{sc} and the largest N_b. The

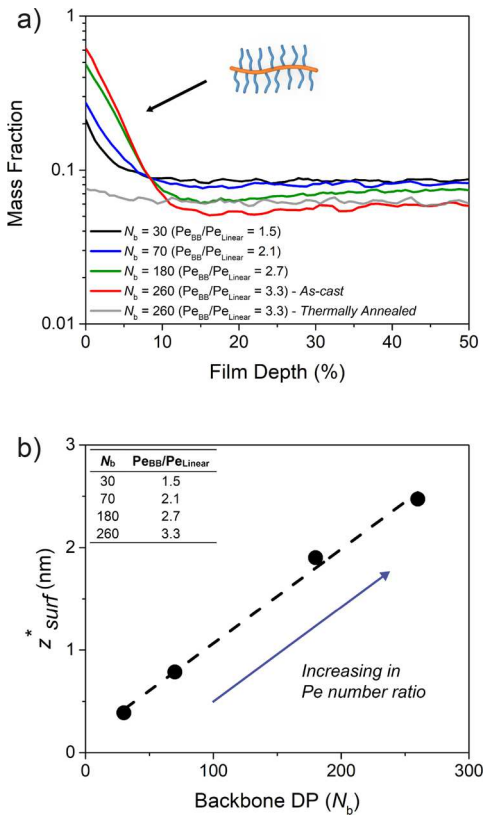

Figure 2. Depth profile analysis and quantification of surface enrichment in blends of BBPS with dPS205 in as-cast films. (a) Mass composition of BBPS with varying N_b as a function of film depth in blend films with dPS205 (N_m/N_{sc} = 4.3). Chlorobenzene was used as a casting solvent (Pe_{Linear} = 1.9). The polymer−air interface and middle of the film are at 0 and 50% film depths, respectively. (b) Surface excess of bottlebrush in the same blend films, calculated from depth profiles shown in (a).

Table 2. Hydrodynamic Radius (R_h) of the Bottlebrush and Linear Polymers

blend	polymer	R_h[a] (nm)	*Pe* ratio[b]
1[c]	BBPS70	10.4	2.12
	dPS205	4.9	
2[d]	BBPS260	16.1	2.15
	dPS548	7.5	
3	BB(PS-*co*-dPS)45	6.1	2.11
	BBPS146	12.9	
4	BB(PS-*co*-dPS)80	8.2	2.17
	BBPS350	17.8	

[a]Measured by GPC viscometry. [b]Péclet number ratio for larger to smaller solutes in each blend. [c]N_m/N_{sc} = 4.3. [d]N_m/N_{sc} = 11.4; the *Pe* number of the smaller particles was greater than 1.9 for all blends and solvents studied.

https://doi.org/10.1021/acs.macromol.2c01418
Macromolecules XXXX, XXX, XXX−XXX

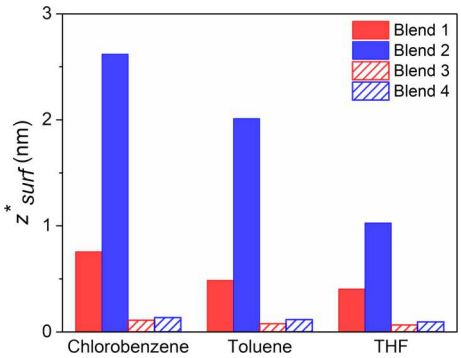

Figure 3. Surface excess of the BBPS when blended with linear dPS (cases 1 and 2) and with BB(PS-*co*-dPS) (cases 3 and 4). Three different casting solvents with different evaporation rates were used to cast the film.

surface excess of the bottlebrush polymer decreased as the backbone length of the bottlebrush polymer and the length of the linear polymer were reduced (blend 1 compared with blend 2). Blends of two bottlebrush polymers having the same N_{sc} and different N_b (blends 3 and 4) showed no preferential enrichment of either component, which we attribute to both polymers having the same chain-end density (set by N_{sc}), which highlights the importance of entropic effects on surface segregation. We also observed an impact of the casting solvent, with the highest surface enrichment observed in films cast from the highest boiling point solvent (chlorobenzene). Since the *Pe* number ratio is approximately the same across all of these samples, it cannot account for variations observed. These measurements indicate that polymer architecture and the solvent evaporation rate all have a significant impact on surface excess in as-cast films, while the *Pe* ratio is not informative.

To further investigate the effect of the solvent evaporation rate, we analyzed thin film blends of BBPS (N_b = 260, N_{sc} = 48) with linear dPS205 (DP = 205, N_m/N_{sc} = 4.3) prepared using four different casting solvents with different evaporation rates (Table 3). In all cases, the weight fraction of the BBPS was 10 wt %, and we analyzed both as-cast and thermally annealed (2 days at 150 °C) blend films. The solvents chosen were all good solvents for polystyrene and had similar solubility parameters (18.2, 19.4, and 19.6 MPa$^{1/2}$ for toluene, THF, and chlorobenzene, respectively[41]). We also found that surface excess of the bottlebrush polymer scaled with solvent volatility and not solubility, which suggests that differences in solvent volatility are more important. In all cases, the BBPS segregated to the film−air interface, but the degree of segregation of the bottlebrush additives to the film surface depended strongly on the evaporation rate of the casting solvent, which might also influence the vitrification of the films. Blend films cast with chlorobenzene exhibited the highest surface concentration (film surface concentration of 62 wt %) while those cast with THF exhibited the lowest surface concentration (26 wt %). Blend films cast with toluene or a 50/50 (mole-to-mole) blend of THF and toluene exhibited surface concentrations between these two limits. Similar trends were observed for the blends with varying N_b (N_b = 30−180), and depth profiles are presented in the Supporting Information, Figure S16. Segregation toward the film−air interface was strongest for higher backbone lengths N_b. We also verified that the differences in segregation behaviors observed for these films were due to solvent evaporation rates by thermally annealing the films at 150 °C for 2 days. As shown in Figure 4b and Supporting Information Figure S17, only very weak segregation toward the film−air interface was observed for thermally annealed films, and the surface excess was independent of the casting solvent in thermally annealed films. This is also reflected in the concentration of the

Table 3. Evaporation Rates for Different Casting Solvents Used in This Study

solvent	saturated vapor pressure at 25 °C (MPa)	evaporation rate (μm/s)[a]	$C_{surf,\ as\text{-}cast}$ (%)[b]	$C_{surf,\ annealed}$ (%)[c]
chlorobenzene	0.0016	3.76	62	7.6
toluene	0.0038	7.46	48	7.8
50/50 THF + toluene	0.0137	13.4	38	8.0
THF	0.0235	18.2	26	8.0

[a]The solvent evaporation rate was measured as described in the Supporting Information. [b]$C_{surf,\ as\text{-}cast}$ is the concentration of the BBPS (N_b = 260) at the surface immediately after casting. Determined by first data point on the ToF-SIMS depth profile (average of three data points). [c]$C_{surf,\ annealed}$ is the concentration of the BBPS (N_b = 260) at the surface after annealing at 150 °C for 2 days. Determined by first data point on the ToF-SIMS depth profile (average of three data points).

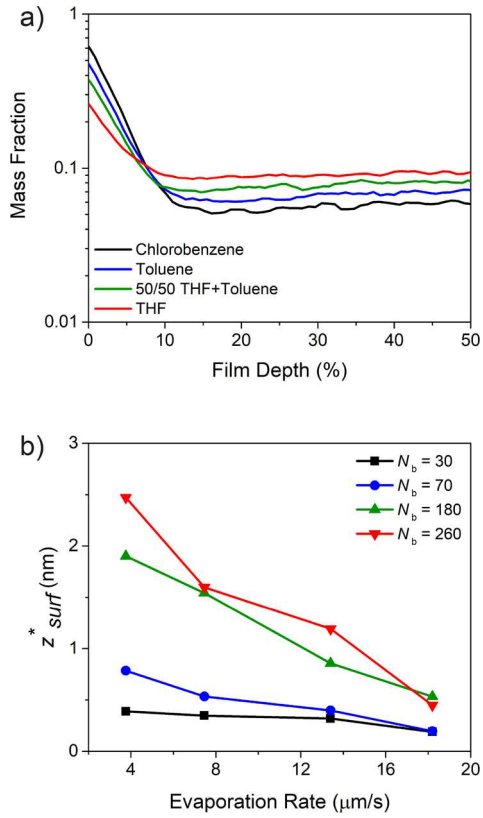

Figure 4. Depth profile analysis and quantification of surface enrichment in blends of bottlebrush polymers with linear polymers. (a) Mass composition of BBPS (N_b = 260) with varying casting solvents as a function of film depth in blend films with linear dPS205 (N_m/N_{sc} = 4.3). The polymer−air interface and middle of the film are at 0 and 50% film depths, respectively. (b) Surface excess as a function of evaporation rate of the casting solvent (as-cast). Four different types of casting solvent were used to prepare the films.

https://doi.org/10.1021/acs.macromol.2c01418
Macromolecules XXXX, XXX, XXX−XXX

bottlebrush at the film surface (Table 3) that decreases significantly after annealing and is independent of the casting solvent. This demonstrates that thermally annealed films have reached the equilibrium state, which is distinct from that after casting.

In prior work, we found that vertical stratification generally does not occur when the length of the linear polymer N_m is less than twice that of the bottlebrush side-chain length. This reflects an entropic preference for short polymers and polymer chain ends near interfaces, but these prior studies did not investigate potential effects of the solvent evaporation rate. To test for segregation of bottlebrush polymers in blends with $N_m/N_{sc} \sim 2$, we prepared blends of BBPS ($N_b = 260$, $N_{sc} = 48$) and linear dPS40 cast from different solvents ($N_m/N_{sc} = 0.8$). Both OM and AFM were used to verify the uniformity of the films, and these data are provided in the Supporting Information, Figures S18 and S19. Depth profiles are presented in the Supporting Information Figure S20. We observed that the casting solvent did not have a significant impact on bottlebrush stratification, with the bottlebrush polymer depleting near the film−air interface. Some stratification was observed toward the substrate interface as the evaporation rate of the casting solvent decreased (Supporting Information Figure S21), but the bottlebrush polymer was depleted near the film−air surface rather than enriched. For blends with $N_m/N_{sc} < 2$, the casting solvent did not have a significant impact on the distribution of the bottlebrush polymer throughout the film, as the bottlebrush was always depleted near the surface. Together with our results for blend films with varying bottlebrush backbone lengths with $N_m/N_{sc} > 4$ (Figures 2 and 4), these results demonstrate that entropic effects contribute for driving bottlebrush additives to the interface during film processing.

Finally, we studied the effect of solvent annealing on the segregation of the bottlebrush polymer. This was motivated by a prior study in which it was hypothesized that segregation of the bottlebrush polymers to interfaces during casting was due in part to the presence of solvent vapors, which can reduce the importance of the polymer−polymer interactions. To test this, we first thermally annealed blend films, resulting in films with BBPS only weakly segregated toward the film−air interface, and then solvent annealed the films. Both OM and AFM were used to verify the uniformity of the films, and these data are provided in the Supporting Information, Figures S22 and S23. As shown in Figure 5 and the Supporting Information Figure S24, in blends of BBPS ($N_b = 180$) and dPS548 (DP = 548, $N_m/N_{sc} = 11.4$) with chlorobenzene as an annealing solvent, solvent annealing significantly increased the concentration of BBPS near the film−air interface. The concentration of BBPS near the film−air interface increased after just 10 min of solvent annealing, and the concentration increased further with 5 h of solvent annealing. Interestingly, solvent annealing was not sufficient to fully recover the enrichment observed in as-cast films, suggesting that other processing effects (e.g., solvent evaporation, solute diffusion) are also important in driving bottlebrush additives toward the film−air interface during film casting. These results demonstrate that solvent annealing can drive bottlebrush additives to the film−air interface.

We hypothesize that segregation of the bottlebrush polymer occurs due to entropic effects that are relevant during solvent evaporation. In solvent-swollen films, polymer−polymer interactions are relatively unimportant due to the presence of solvent, and the bottlebrush polymers segregate to the film surface due to more favorable entropic effects. Stronger surface segregation is observed for higher boiling point solvents, as there is more time for the bottlebrush to diffuse to the interface and vitrification of the film is delayed due to slower evaporation. Film drying, which starts at the top and progresses through the film, effectively arrests polymer diffusion, resulting in bottlebrush polymers enriched at the top surface of the film. In dry films, polymer−polymer interactions become more important, and it is favorable for the bottlebrush additives to migrate to the bulk film and increase the entropy of mixing.

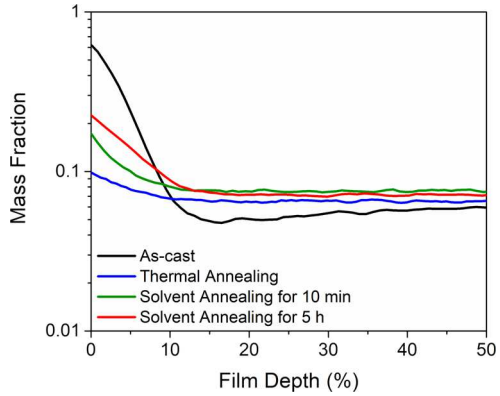

Figure 5. Mass composition of BBPS ($N_b = 180$) as a function of film depth in blend films with linear dPS548 ($N_m/N_{sc} = 11.4$). The polymer−air interface and middle of the film are at 0 and 50% film depths, respectively.

■ CONCLUSIONS

We studied the blend system of BBPS and linear dPS to understand processing effects on surface segregation of bottlebrush polymers. In our studies, the *Pe* number was systematically varied through changes in bottlebrush backbone length (N_b) and solvent evaporation rate. In contrast to other binary blend systems, such as colloid/colloid, polymer/colloid, and polymer/polymer, variations in the *Pe* number by itself were not predictive of vertical stratification of the blends. Instead, we found that the degree of surface excess increases with length of the bottlebrush backbone (N_b). Enrichment of the bottlebrush near the film−air interface was only observed for $N_m/N_{sc} > 2$, pointing to an entropically mediated segregation during processing. We also tested four different casting solvents with varying evaporation rates, and stronger surface excess was observed as the evaporation rate of the casting solvent decreased. Finally, to explain the excessive surface segregation of bottlebrush polymers during casting state, we studied the effect of the solvent annealing on the segregation of the bottlebrush polymer. We also found that we could reversely control the vertical stratification behavior by solvent annealing the film and the surface enrichment of the bottlebrush depended on the solvent annealing times. These results demonstrate that bottlebrush additives migrate where there is a favorable entropic attraction, and processing can enhance the degree of surface enrichment. This work can also lead to new approaches for tailoring surface properties of polymeric materials.

■ ASSOCIATED CONTENT

Supporting Information

The Supporting Information is available free of charge at https://pubs.acs.org/doi/10.1021/acs.macromol.2c01418.

^{1}H NMR and GPC characterization, polymer film thickness, details on methods for ToF-SIMS calibration, hydrodynamic radius (R_h) of bottlebrush and linear polymers, schematic of the BBPS and BB(PS-*co*-dPS) synthesis method, OM images of the polymer film, AFM analysis of the polymer film, calibrated and uncalibrated full-depth profiles of the polymer blends, detailed description of calculating the evaporation rate of the solvent, and surface excess of the BBPS/dPS blends after thermal annealing (PDF)

■ AUTHOR INFORMATION

Corresponding Authors

Gila E. Stein − *Department of Chemical and Biomolecular Engineering, University of Tennessee, Knoxville, Tennessee 37996, United States;* orcid.org/0000-0002-3973-4496; Email: gstein4@utk.edu

Rafael Verduzco − *Department of Chemical and Biomolecular Engineering and Department of Materials Science and NanoEngineering, Rice University, Houston, Texas 77005, United States;* orcid.org/0000-0002-3649-3455; Email: rafaelv@rice.edu

Authors

Dongjoo Lee − *Department of Chemical and Biomolecular Engineering, Rice University, Houston, Texas 77005, United States*

Nilesh Charpota − *Department of Chemical and Biomolecular Engineering, University of Tennessee, Knoxville, Tennessee 37996, United States*

Hao Mei − *Department of Chemical and Biomolecular Engineering, Rice University, Houston, Texas 77005, United States*

Tanguy Terlier − *SIMS Lab, Shared Equipment Authority, Rice University, Houston, Texas 77005, United States*

Danica Pietrzak − *Department of Chemical and Biomolecular Engineering, Rice University, Houston, Texas 77005, United States*

Complete contact information is available at: https://pubs.acs.org/10.1021/acs.macromol.2c01418

Notes

The authors declare no competing financial interest.

■ ACKNOWLEDGMENTS

D.L., H.M., and R.V. acknowledge support from the National Science Foundation under Grant No. CMMI-1934045. N.C. and G.E.S. acknowledge support from the National Science Foundation under Grant No. CMMI-1934061. ToF-SIMS analyses were carried out with support provided by the National Science Foundation under Grant No. CBET-1626418. This work was conducted in part using resources of the Shared Equipment Authority at Rice University.

■ REFERENCES

(1) Stein, G. E.; Laws, T. S.; Verduzco, R. Tailoring the Attraction of Polymers toward Surfaces. *Macromolecules* **2019**, *52*, 4787−4802.

(2) Nemani, S. K.; Annavarapu, R. K.; Mohammadian, B.; Raiyan, A.; Heil, J.; Haque, M. A.; Abdelaal, A.; Sojoudi, H. Surface Modification of Polymers: Methods and Applications. *Adv. Mater. Interfaces* **2018**, *5*, 1801247.

(3) Ma, S.; Zhang, X.; Yu, B.; Zhou, F. Brushing up Functional Materials. *NPG Asia Mater.* **2019**, *11*, 24.

(4) Mozetič, M. Surface Modification to Improve Properties of Materials. *Materials* **2019**, *12*, 441.

(5) Penn, L. S.; Wang, H. Chemical Modification of Polymer Surfaces: A Review. *Polym. Adv. Technol.* **1994**, *5*, 809−817.

(6) Discekici, E. H.; Pester, C. W.; Treat, N. J.; Lawrence, J.; Mattson, K. M.; Narupai, B.; Toumayan, E. P.; Luo, Y.; McGrath, A. J.; Clark, P. G.; Read de Alaniz, J.; Hawker, C. J. Simple Benchtop Approach to Polymer Brush Nanostructures Using Visible-Light-Mediated Metal-Free Atom Transfer Radical Polymerization. *ACS Macro Lett.* **2016**, *5*, 258−262.

(7) Fromel, M.; Sweeder, D. M.; Jang, S.; Williams, T. A.; Kim, S. H.; Pester, C. W. Superhydrophilic Polymer Brushes with High Durability and Anti-Fogging Activity. *ACS Appl. Polym. Mater.* **2021**, *3*, 5291−5301.

(8) Kim, H. T.; Jeong, O. C. PDMS Surface Modification Using Atmospheric Pressure Plasma. *Microelectron. Eng.* **2011**, *88*, 2281−2285.

(9) Sharma, V.; Dhayal, M.; Govind; Shivaprasad, S. M.; Jain, S. C. Surface Characterization of Plasma-Treated and PEG-Grafted PDMS for Micro Fluidic Applications. *Vacuum* **2007**, *81*, 1094−1100.

(10) Asatekin, A.; Barr, M. C.; Baxamusa, S. H.; Lau, K. K. S.; Tenhaeff, W.; Xu, J.; Gleason, K. K. Designing Polymer Surfaces via Vapor Deposition. *Mater. Today* **2010**, *13*, 26−33.

(11) Cho, Y.; Lee, M.; Park, S.; Kim, Y.; Lee, E.; Im, S. G. A Versatile Surface Modification Method via Vapor-Phase Deposited Functional Polymer Films for Biomedical Device Applications. *Biotechnol. Bioprocess Eng.* **2021**, *26*, 165−178.

(12) Ding, Y. H.; Floren, M.; Tan, W. Mussel-Inspired Polydopamine for Bio-Surface Functionalization. *Biosurface Biotribol.* **2016**, *2*, 121−136.

(13) Asatekin, A.; Kang, S.; Elimelech, M.; Mayes, A. M. Anti-Fouling Ultrafiltration Membranes Containing Polyacrylonitrile-Graft-Poly(Ethylene Oxide) Comb Copolymer Additives. *J. Membr. Sci.* **2007**, *298*, 136−146.

(14) Maguire, S. M.; Boyle, M. J.; Bilchak, C. R.; Demaree, J. D.; Keller, A. W.; Krook, N. M.; Ohno, K.; Kagan, C. R.; Murray, C. B.; Rannou, P.; Composto, R. J. Grafted Nanoparticle Surface Wetting during Phase Separation in Polymer Nanocomposite Films. *ACS Appl. Mater. Interfaces* **2021**, *13*, 37628−37637.

(15) Zhang, R.; Lee, B.; Stafford, C. M.; Douglas, J. F.; Dobrynin, A. V.; Bockstaller, M. R.; Karim, A. Entropy-Driven Segregation of Polymer-Grafted Nanoparticles under Confinement. *Proc. Natl. Acad. Sci. U. S. A.* **2017**, *114*, 2462−2467.

(16) Gibson, C. P.; Litwinowicz, M. A.; Tellam, J. P.; Welbourn, R. J. L.; Skoda, M. W. A.; Claussen, J.; Thompson, R. L. Water-Resistant Surface Modification of Hydrophobic Polymers with Water-Soluble Surfactant Additives. *Polymer* **2021**, *13*, 3407.

(17) Gökaltun, A.; Kang, Y. B.; Yarmush, M. L.; Usta, O. B.; Asatekin, A. Simple Surface Modification of Poly(Dimethylsiloxane) via Surface Segregating Smart Polymers for Biomicrofluidics. *Sci. Rep.* **2019**, *9*, 7377.

(18) Hester, J. F.; Banerjee, P.; Mayes, A. M. Preparation of Protein-Resistant Surfaces on Poly(Vinylidene Fluoride) Membranes via Surface Segregation. *Macromolecules* **1999**, *32*, 1643.

(19) Mah, A. H.; Laws, T.; Li, W.; Mei, H.; Brown, C. C.; Ievlev, A.; Kumar, R.; Verduzco, R.; Stein, G. E. Entropic and Enthalpic Effects in Thin Film Blends of Homopolymers and Bottlebrush Polymers. *Macromolecules* **2019**, *52*, 1526−1535.

(20) Mitra, I.; Li, X.; Pesek, S. L.; Makarenko, B.; Lokitz, B. S.; Uhrig, D.; Ankner, J. F.; Verduzco, R.; Stein, G. E. Thin Film Phase Behavior of Bottlebrush/Linear Polymer Blends. *Macromolecules* **2014**, *47*, 5269−5276.

(21) Walton, D. G.; Soo, P. P.; Mayes, A. M.; Allgor, S. J. S.; Fujii, J. T.; Griffith, L. G.; Ankner, J. F.; Kaiser, H.; Johansson, J.; Smith, G. D.; Barker, J. G.; Satija, S. K. Creation of Stable Poly(Ethylene Oxide) Surfaces on Poly(Methyl Methacrylate) Using Blends of Branched and Linear Polymers. *Macromolecules* **1997**, *30*, 6947−6956.

(22) Mei, H.; Laws, T. S.; Mahalik, J. P.; Li, J.; Mah, A. H.; Terlier, T.; Bonnesen, P.; Uhrig, D.; Kumar, R.; Stein, G. E.; Verduzco, R.

Entropy and Enthalpy Mediated Segregation of Bottlebrush Copolymers to Interfaces. *Macromolecules* **2019**, *52*, 8910−8922.
(23) Miyagi, K.; Mei, H.; Terlier, T.; Stein, G. E.; Verduzco, R. Analysis of Surface Segregation of Bottlebrush Polymer Additives in Thin Film Blends with Attractive Intermolecular Interactions. *Macromolecules* **2020**, *53*, 6720.
(24) Mei, H.; Mahalik, J. P.; Lee, D.; Laws, T. S.; Terlier, T.; Stein, G. E.; Kumar, R.; Verduzco, R. Understanding Interfacial Segregation in Polymer Blend Films with Random and Mixed Side Chain Bottlebrush Copolymer Additives. *Soft Matter* **2021**, *17*, 9028−9039.
(25) Pesek, S. L.; Lin, Y.-H.; Mah, H. Z.; Kasper, W.; Chen, B.; Rohde, B. J.; Robertson, M. L.; Stein, G. E.; Verduzco, R. Synthesis of Bottlebrush Copolymers Based on Poly(Dimethylsiloxane) for Surface Active Additives. *Polymer* **2016**, *98*, 495−504.
(26) Yethiraj, A. Entropic and Enthalpic Surface Segregation from Blends of Branched and Linear Polymers. *Phys. Rev. Lett.* **1995**, *74*, 2018−2021.
(27) Lee, J. S.; Lee, N.-H.; Peri, S.; Foster, M. D.; Majkrzak, C. F.; Hu, R.; Wu, D. T. Surface Segregation Driven by Molecular Architecture Asymmetry in Polymer Blends. *Phys. Rev. Lett.* **2014**, *113*, No. 225702.
(28) He, Q.; Wang, S.-F.; Hu, R.; Akgun, B.; Tormey, C.; Peri, S.; Wu, D. T.; Foster, M. D. Evidence and Limits of Universal Topological Surface Segregation of Cyclic Polymers. *Phys. Rev. Lett.* **2017**, *118*, No. 167801.
(29) Zhou, J.; Man, X.; Jiang, Y.; Doi, M. Structure Formation in Soft-Matter Solutions Induced by Solvent Evaporation. *Adv. Mater.* **2017**, *29*, 1703769.
(30) Schulz, M.; Keddie, J. L. A Critical and Quantitative Review of the Stratification of Particles during the Drying of Colloidal Films. *Soft Matter* **2018**, *14*, 6181−6197.
(31) Cheng, S.; Grest, G. S. Dispersing Nanoparticles in a Polymer Film via Solvent Evaporation. *ACS Macro Lett.* **2016**, *5*, 694−698.
(32) Fortini, A.; Martín-Fabiani, I.; De La Haye, J. L.; Dugas, P.-Y.; Lansalot, M.; D'Agosto, F.; Bourgeat-Lami, E.; Keddie, J. L.; Sear, R. P. Dynamic Stratification in Drying Films of Colloidal Mixtures. *Phys. Rev. Lett.* **2016**, *116*, No. 118301.
(33) Fortini, A.; Sear, R. P. Stratification and Size Segregation of Ternary and Polydisperse Colloidal Suspensions during Drying. *Langmuir* **2017**, *33*, 4796−4805.
(34) Howard, M. P.; Nikoubashman, A.; Panagiotopoulos, A. Z. Stratification Dynamics in Drying Colloidal Mixtures. *Langmuir* **2017**, *33*, 3685−3693.
(35) Howard, M. P.; Nikoubashman, A.; Panagiotopoulos, A. Z. Stratification in Drying Polymer−Polymer and Colloid−Polymer Mixtures. *Langmuir* **2017**, *33*, 11390−11398.
(36) Lee, K.; Choi, S. Q. Stratification of Polymer−Colloid Mixtures *via* Fast Nonequilibrium Evaporation. *Soft Matter* **2020**, *16*, 10326−10333.
(37) Radzinski, S. C.; Foster, J. C.; Matson, J. B. Preparation of Bottlebrush Polymers via a One-Pot Ring-Opening Polymerization (ROP) and Ring-Opening Metathesis Polymerization (ROMP) Grafting-Through Strategy. *Macromol. Rapid Commun.* **2016**, *37*, 616−621.
(38) Stafford, C. M.; Roskov, K. E.; Epps, T. H.; Fasolka, M. J. Generating Thickness Gradients of Thin Polymer Films via Flow Coating. *Rev. Sci. Instrum.* **2006**, *77*, No. 023908.
(39) Trueman, R. E.; Lago Domingues, E.; Emmett, S. N.; Murray, M. W.; Keddie, J. L.; Routh, A. F. Autostratification in Drying Colloidal Dispersions: Experimental Investigations. *Langmuir* **2012**, *28*, 3420−3428.
(40) Makepeace, D. K.; Fortini, A.; Markov, A.; Locatelli, P.; Lindsay, C.; Moorhouse, S.; Lind, R.; Sear, R. P.; Keddie, J. L. Stratification in Binary Colloidal Polymer Films: Experiment and Simulations. *Soft Matter* **2017**, *13*, 6969−6980.
(41) Fried, J. R. *Polymer Science and Technology*; 3rd ed.; Prentice Hall: Upper Saddle River, NJ, 2014.

https://doi.org/10.1021/acs.macromol.2c01418
Macromolecules XXXX, XXX, XXX−XXX